Indirect nanoplasmonic sensing

B. Demirdjian, Igor Ozerov, F. Bedu, A. Ranguis, Claude R Henry

Indirect nanoplasmonic sensing.

B. Demirdjian, I. Ozerov, A. Ranguis, F. Bedu, C. R. Henry

Aix-Marseille University, CNRS, CINaM UMR 7325, 13288 Marseille, France

SCIENTIFIC BACKGROUND

Development of chemical and biological nanosensors based on the extraordinary optical properties of noble-metal nanoparticles.

Nanosensors based on localized surface plasmon resonance (LSPR) are sensitive to small local changes in refractive index at the surface of metal nanoparticles during the adsorption/desorption of molecules.
➔ These changes induce a shift in the wavelength of the LSPR response.

Variations of the LSPR peak extinction is linked to the collective oscillation of electrons in the metal. The minimum of reflection corresponds to a maximum of absorption.

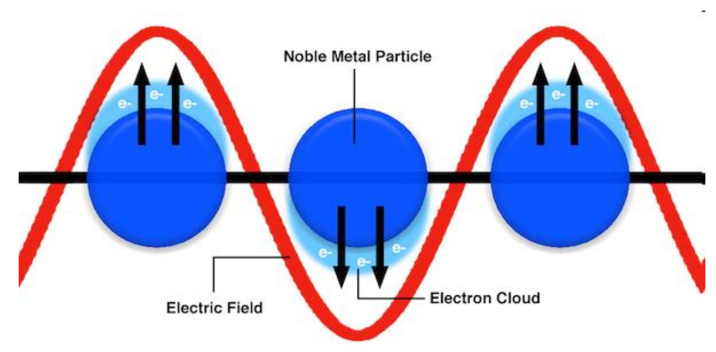

Figure: http://simslab.uwaterloo.ca/research/biomems-sensors.php

INDIRECT NANOPLASMONIC SENSING (INPS)

Gas adsorption on nanoparticles modify their surface dielectric properties

➔ a shift in the wavelength of the LSPR response of the underlying gold disk detector.

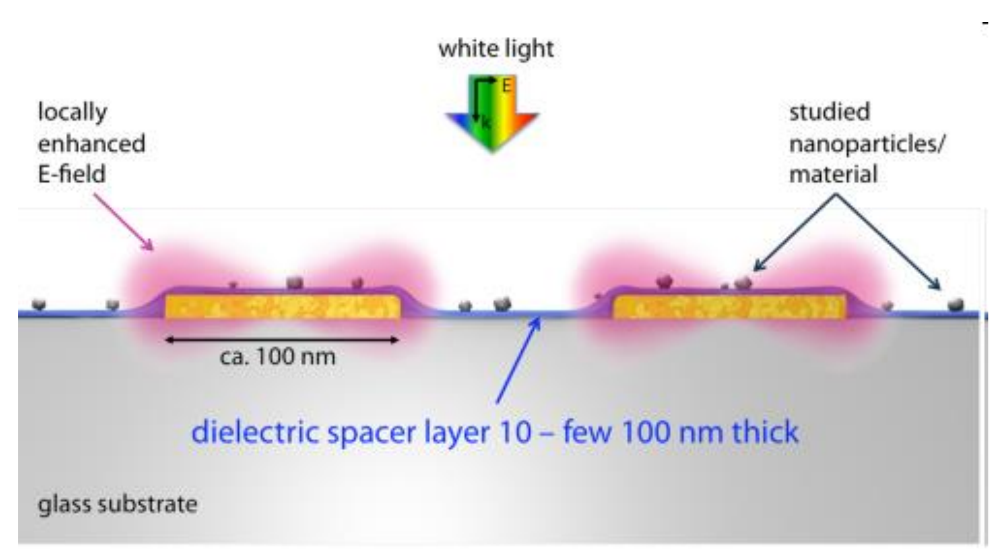

http://www.insplorion.com/technology/indirect-nanoplasmonic-sensing

GOLD NANODISKS FABRICATION: EBL PROCESS

Sample holder = borosilicate glass window, e = 1 mm, Ø = 25,4 mm
Cleaning: acetone + US, then isopropanol + US, EDI rinsing,
oxygen plasma oven at 150°C (300 W during 10 min)

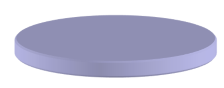

PMMA spin-coating (resin 950 K at 4 %, speed : 4000 rpm, e = 270 nm
annealing 10 min at 170°C)

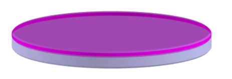

Gold layer deposition (5 nm)
to remove the charges (Edwards 306)

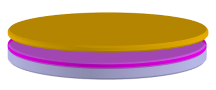

The gold film is irradiated with an electron beam (Raith PIONNEER)
Area of 1 x 1 mm2

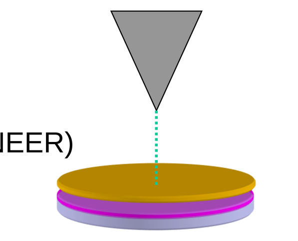

Revelation in acetone (Au is removed) then with MIBK/IPA 1 : 3 during 45 s
Then with IPA during 45 s (➔ holes in the resin)

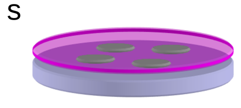

Cr and Au evaporation within the PMMA resin (Edwards 306)
e_{Cr} = 2 nm, e_{Au} = 20 nm
Lift-off of the resin (acetone + US)

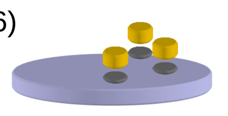

➔ Precise control of the shape, the size and the pitch of gold nanodisks

LSPR MEASUREMENTS: EXPERIMENTAL SET-UP

"Avasoft-Full" software on a laptop

UV-VIS spectrometer (CCD detector, Avantes, AvaSpec-ULS3648-USB2)

F.O. (Avantes FC-IR200-2) + collimating lens (Avantes, COL-UV/VIS)

Tungsten halogen source (Avantes, AvaLight-HAL-S)

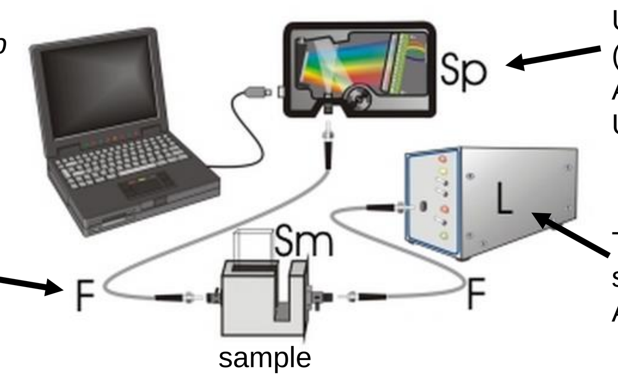

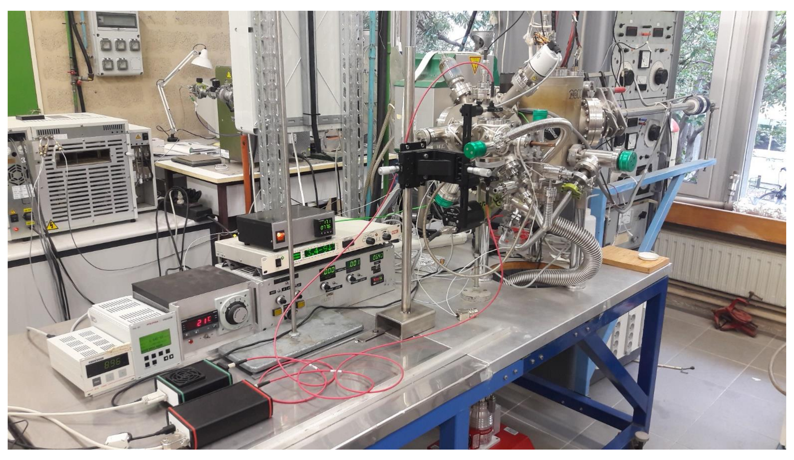

The INPS UHV experimental set up

The sample holder

OPTIMISATION OF THE GOLD NANODISKS PARAMETERS

FDTD simulations ➔ best theoretical LSPR S/N signals obtained with the biggest aspect ratio *ie* the biggest diameter (for a given h)

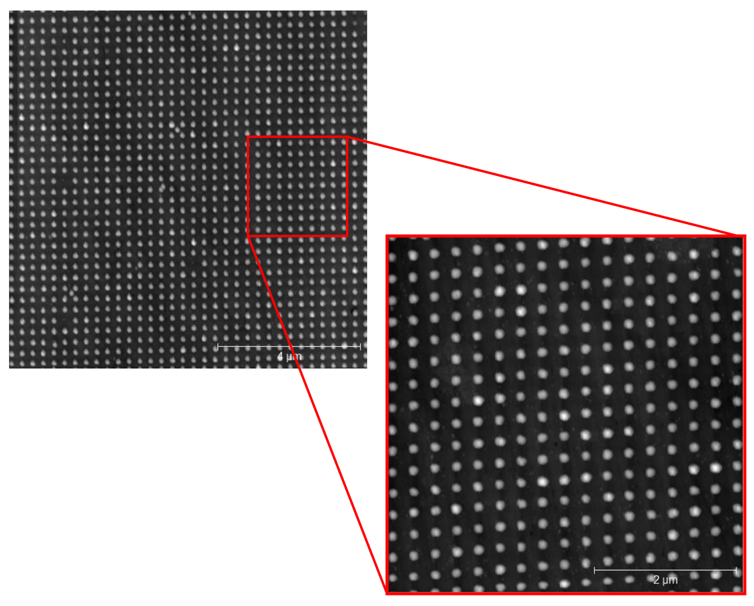

Tapping mode topographical AFM images of gold nanodisks on borosilicate window (images obtained with a PSIA apparatus XE-100)

<p> = 300 nm

<h> = 29 nm,

d = 100, 150 nm

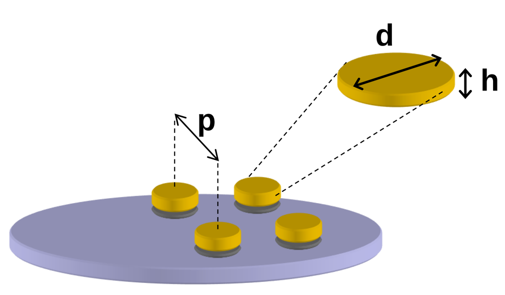

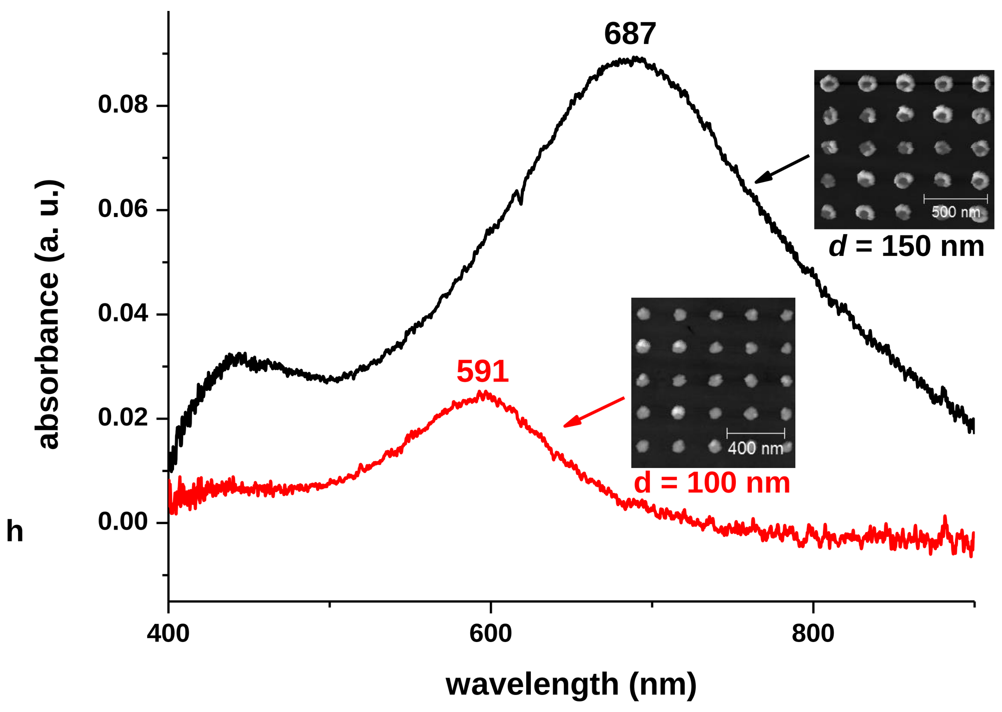

Experimental LSPR responses for gold nanodisks deposited onto a borosilicate glass window vs the diameter, d. Tapping mode topographical AFM images of gold nanodisks with d = 100 and 150 nm. Images obtained with a PSIA XE-100.

SOOT DEPOSITION ON GOLD NANODISKS: DROPLET DEPOSITION

Soot particles are involved in several atmospheric processes (ice nuclei, contrails formation, radiative forcing, chemical reactions…), it is important to well characterize the water/soot interaction mechanism

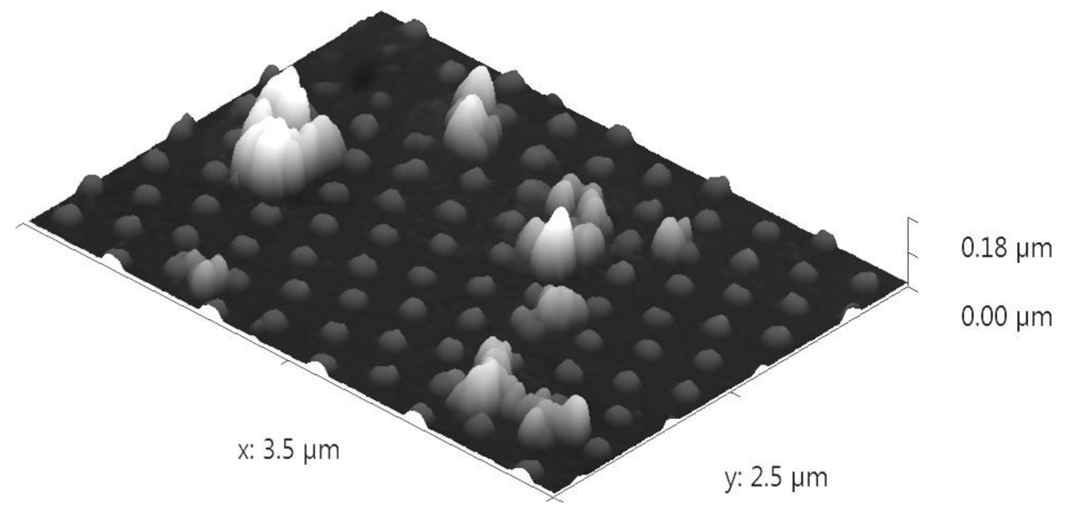

Tapping mode topographical AFM image of AEC soot particles deposited on gold nanodisks (covered by a SiO_2 layer). Image obtained with a PSIA apparatus (XE-100).

RESPONSE OF THE LSPR NANOSENSORS

The response of LSPR nanosensors follows a simple model described by the group of Campbell:

$$\Delta\lambda = m\,(n_2-n_1)\,[1 - \exp(-2d/l_d)] \qquad (1)$$

Δλ: wavelength shift
m: sensitivity of the refractive index (RI)
n_2 and n_1: RIs of different surrounding media
d: effective thickness of the adsorbate layer
l_d: characteristic decay length of the evanescent electromagnetic field.

REFERENCE : WATER ADSORPTION ON SiO_2 / GOLD DISKS

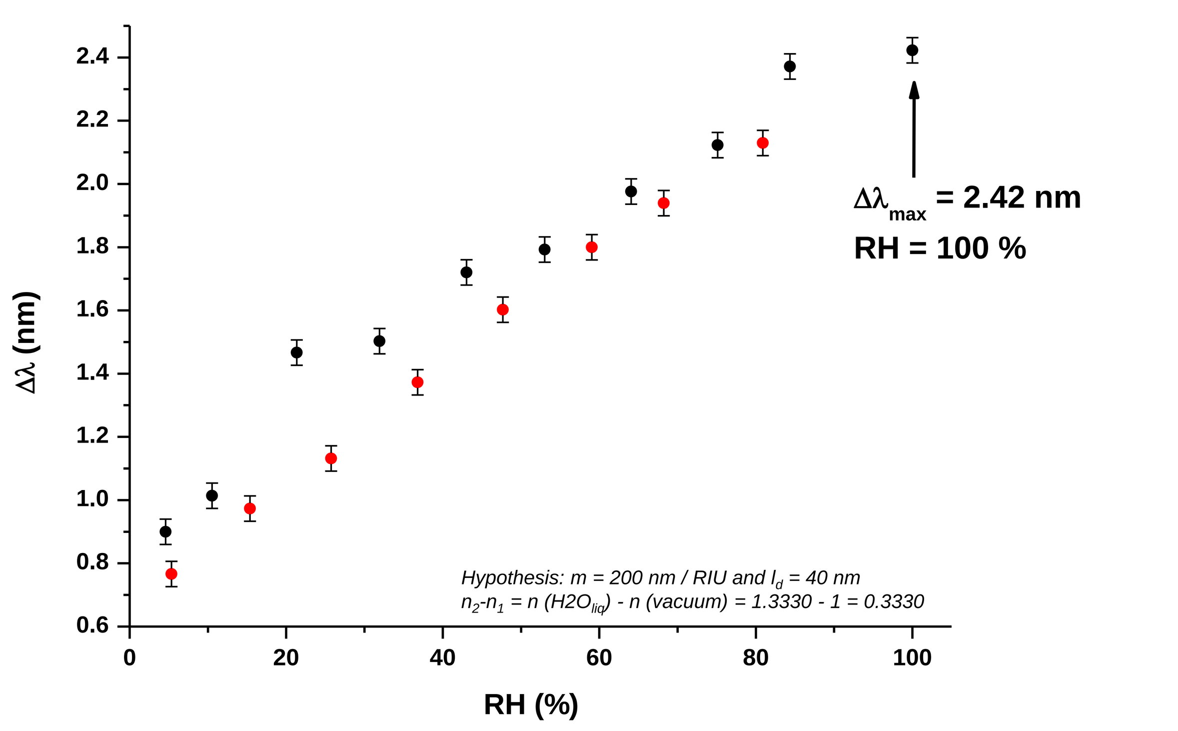

Evolution of the shift Δλ of the LSPR response versus the relative humidity inside the reactor at room temperature during the adsorption of water vapor on the gold nanodisks covered by a SiO_2 layer. Black dots are obtained during the adsorption, and red dots are obtained during the desorption. Error bars are indicated.

Δλ is almost linear *vs* the relative humidity, at RH = 100%, Δλ = $\Delta\lambda_{max}$ = 2.42 nm.
➔ water layer thickness d = 0.67 nm (~ 2.2 water ML) Equation (1)

Good reversibility of the adsorption and desorption curves (H_2O physisorption and no chemisorption of water molecules on SiO_2)

Highly sensitive sensor: accuracy of the wavelength measurement in the LSPR response is 0.04 nm ➔ detection of about 2/100 of water ML !

WATER ADSORPTION ON HYDROPHOBIC SOOT PARTICLES

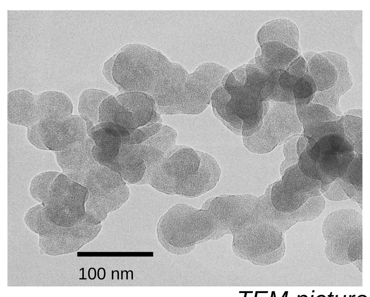

TEM picture

Hydrophobic soot
(laboratory lamp soot)

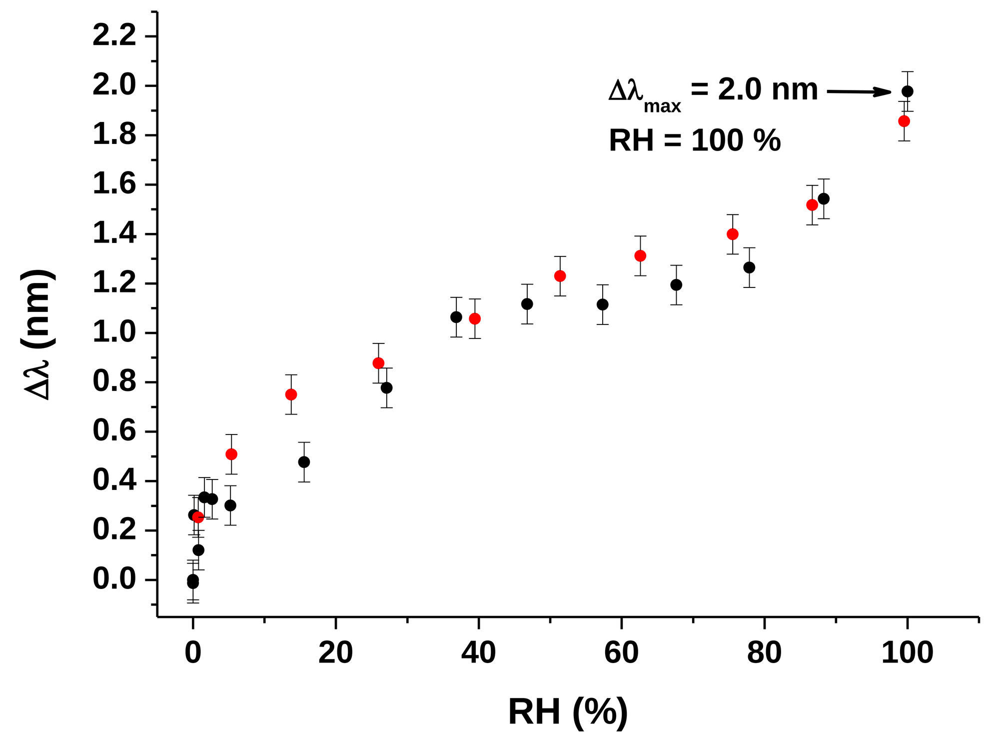

Evolution of the shift Δλ of the LSPR response versus the relative humidity inside the reactor at room temperature during the adsorption of water vapor on soot particles deposited on gold nanodisks covered by a SiO_2 layer. Black dots are obtained during the adsorption, and red dots are obtained during the desorption. Error bars are indicated.

BLUE SHIFT ? ➔ MODELISATION (A. KARAPETYAN)

Hydrophilic soot aggregates collapse into + dense structures during RH ↗ (Mikhailov):
➔ RH = 100 % soot aggregates are more compact
- higher mass fractal dimension Df
- smaller gyration radius
- higher n and k values

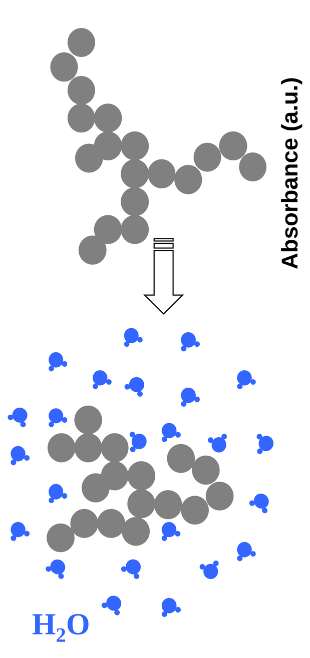

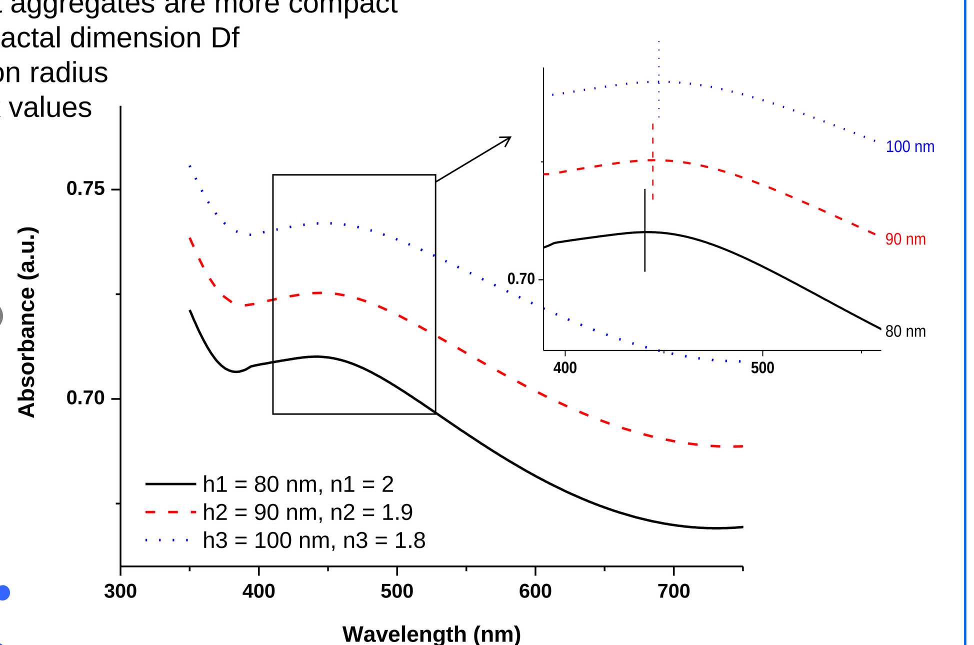

Absorbance of the thin multilayers system (C/SiO_2/gold/glass) as a function of the incident wavelength. k = 0.75 for the three thicknesses. Analytical Born and Wolf equations.

From 100 to 90 nm
➔ Δλ = - 4 nm
From 90 to 80 nm
➔ Δλ = - 3 nm

WATER ADSORPTION ON HYDROPHILIC SOOT PARTICLES

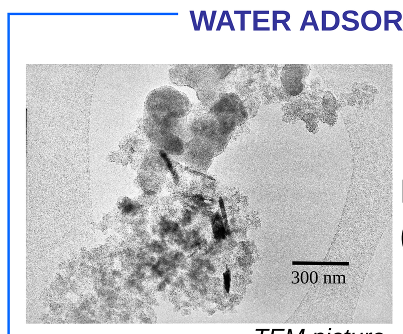

TEM picture

Hydrophilic soot
(aircraft engine combustor soot)

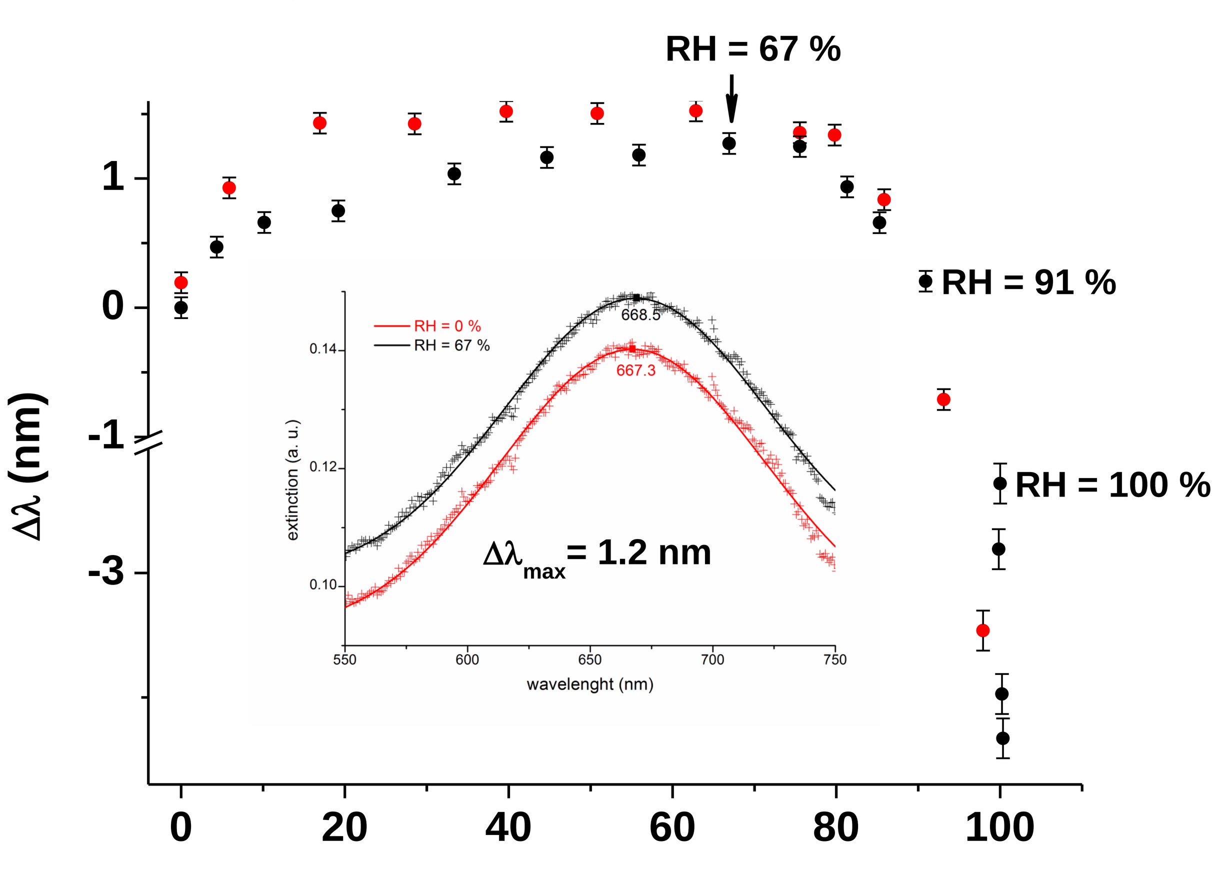

Evolution of the shift Δλ of the LSPR response versus the relative humidity inside the reactor at room temperature during the adsorption of water vapor on soot particles deposited on gold nanodisks covered by a SiO_2 layer. Black dots are obtained during the adsorption, and red dots are obtained during the desorption. Error bars are indicated.

➔ Peculiar and reversible blue-shift !

CONLUSIONS AND OUTLOOKS

Conclusions

➔ High sensitive water sensor (detection of a few hundredths of H_2O ML)
➔ Detect morphology changes of soot aggregates
➔ Large (P, T) domains of studies
➔ Non destructive probe

Outlooks

➔ Quantitive measurements with mass spectrometry

➔ Continuing FDTD simulations

➔ Chemical reactivity gas / nanoparticles:

•Catalysis
Metallic nanoparticles (Pt, Pd, …) + CO, O_2 + H_2, NO_x

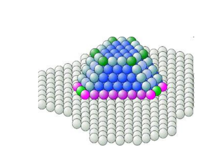

•Environmental heterogenous reactions
Ice nucleation on soot particles
Photochemistry and reactivity NO_2/soot ➔ O_3

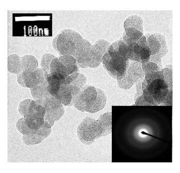

BIBLIOGRAPHY

Bond, T. C.; Doherty, S. J.; Fahey, D. W.; Forster, P. M.; Berntsen, T.; De Angelo, B. J.; Flanner, M. G.; Ghan, S.; Kärcher, B.; Koch, D. Bounding the role of black carbon in the climate system: a scientific assessment. J. Geophys. Res. **2013**, 118, 5380–5552.
Kahnert, M. Modelling the optical and radiative properties of freshly emitted light absorbing carbon within an atmospheric chemical transport model. Atmos. Chem. Phys. **2010**, 10, 1403–1416.
Liu, L.; Mishchenko, M. I. Effects of aggregation on scattering and radiative properties of soot aerosols. J Geophys. Res. **2005**, 110, D11211.
Carrico, C. M.; Petters, M. D.; Kreidenweis, S. M.; Sullivan, A. P.; McMeeking, G. R.; Levin, E. J. T.; Engling, G.; Malm, W. C.; Collett Jr., J. L. Water uptake and chemical composition of fresh aerosols generated in open burning of biomass. Atmos. Chem. Phys. **2010**, 10, 5165–5178.
Cheng, T.; Gu, X.; Yu, W.; Hao, C. Effects of atmospheric water on the optical properties of soot aerosols with different mixing states. Journal of Quantitative Spectroscopy and Radiative Transfer **2014**, 147, 196-206.
Mikhailov, E. F.; Vlasenko, S. S.; Podgorny, I. A.; Ramanathan, V.; Corrigan, C. E. Optical properties of soot–water drop agglomerates: an experimental study. J Geophys. Res. **2006**, 111, D07209.
Barbillon, G.; Bijeon, J.-L.; Bouillard, J.-S.; Plain, J.; Lamy de la Chapelle, M.; Adam, P.-M.; Royer, P. Detection in near-field domain of biomolecules adsorbed on a single metallic nanoparticle. J. Microsc. **2008**, 229, 270−274.
Larsson, E. M.; Langhammer, C.; Zoric, I.; Kasemo, B. Nanoplasmonic probes of catalytic reactions. Science **2009**, 326, 1091-1094.
Jung, L. S.; Campbell, C. T.; Chinowsky, T. M.; Mar, M. N.; Yee, S. S. Quantitative interpretation of the response of surface plasmon resonance sensors to adsorbed films. Langmuir **1998**, 14, 5636−5648.
Born, M.; Wolf, E. Principles of Optics, 7th Edition; Cambridge University Press: Cambridge, U.K., **1999**.
B. Demirdjian, F. Bedu, A. Ranguis, I. Ozerov, A. Karapetyan, C.R. Henry. Indirect Nanoplasmonic Sensing to Probe with a High Sensitivity the Interaction of Water Vapor with Soot Aerosols. The Journal of Physical Chemistry Letters **2015**, 6, 4148-4152.
B. Demirdjian, F. Bedu, A. Ranguis, I. Ozerov, C.R. Henry. Water adsorption by a sensitive calibrated gold plasmonic nanosensor. Langmuir **2018,** 34, 5381-5385.